Full Paper

Propellants, Explosives, Pyrotechnics

DOI: 10.1002/prep.201500187

Nanostructuring of Pure and Composite-Based K6 Formulations with Low Sensitivities

Lucia Blas,*[a] Martin Klaumünzer,[a] Florent Pessina,[a] Silke Braun,[b] and Denis Spitzer[a]

Abstract: The aim of this work was to desensitize keto-RDX, respectively 2-oxo-1,3,5-trinitro-1,3,5-triazacyclohexane (K6). For this purpose, two different methods were employed. First, nano-K6 was produced by means of the Spray Flash Evaporation process. Particles with a median size of 74 nm were obtained. Sensitivity to friction and electrostatic discharge were reduced by downscaling particle size of K6. Second, due to their molecular analogy, the mixing of K6 and RDX was studied. For that reason, a physical nanometric mixture of K6 and RDX was produced by the same technique. In the latter case, an inter-particular synergy between both compounds was noticed but without forming a cocrystal. The median particle size of the mixture is about 82 nm, and its sensitivity is between the ones of raw nanomaterials concerning friction and electrostatic discharge. Moreover, the mixture is less sensitive to impact (3.03 J) than nano-K6 ($<$ 1.56 J) and nano-RDX (threshold is 2.0 J).

Keywords: Spray Flash Evaporation · Energetic nanomaterials · Nano-K6 · Nano-K6/nano-RDX mixture · Desensitization

1 Introduction

Over the last years, the use of nanotechnology has provided an important advance in the field of energetic materials. Several promising effects of nanostructured energetic materials have been revealed, for instance, less sensitivity to external stimuli and higher performances [1,2]. Previous studies have shown that sensitivity of nitramine explosives (e.g. RDX, HMX, and CL-20) is intensely affected by their individual particle size distribution [3,4]. By decreasing the particle size of an explosive, the formation of intracrystalline heterogeneities (voids, crystallographic defects, gaseous or liquid inclusions, and impurities) is reduced, and consequently the formation of "hot spots", which start the accidental ignition reaction chain, can be suppressed. For this reason, many recent studies in the literature were focused on the production of energetic nanomaterials, such as n-RDX [5–7], n-HMX [8–10], and n-CL-20 [11,12].

The production of nanostructured energetic materials has been accomplished by dissolution and recrystallization or by grinding the explosive that means by bottom up or top down techniques. Within grinding methods (e.g. wet milling [13]), particles are subjected to high levels of mechanical stress, and structural elements of the solid are broken. In contrast, dissolution and the subsequent recrystallization potentially allows crystals to grow free of stress. Methods included in this category are sol-gel processes [12], vacuum-condensation [14], electrospray [15], ultrasound assisted nanocrystallization, and Rapid Expansion of Supercritical Solutions (RESS) [5]. These techniques are discontinuous or expensive processes, therefore they are not suitable for industrial production. Risse et al. proposed the Spray Flash Evaporation (SFE) for continuous nanostructured particles production [16,17]. The latter represents an effective and innovative process that consists in heating up a solution of the energetic material and exposing it to an important and high pressure drop. Subsequently the solvent evaporates immediately, the dissolved material completely crystallizes and is recovered by cyclones as a dry ultrafine powder. This specific technique has been used successfully to produce n-HMX [10] and moreover, to produce nanometric cocrystals for medical or energetic applications [18].

Mixtures of explosives (as hexolite RDX/TNT, octol TNT/HMX, or pentolite TNT/PETN) have been developed and used for different applications during last decades [19]. These mixtures can present different properties compared to original pure single compounds (thermal stability, sensitivity…) [20]. Moreover, the cocrystal formation between different explosives has been revealed as an interesting way to obtain energetic materials with enhanced performances, combining high reactivity with significantly reduced sensitivity.

[a] *L. Blas, M. Klaumünzer, F. Pessina, D. Spitzer*
NS3E Nanomatériaux pour les Systèmes Sous Sollicitations Extrêmes UMR 3208 ISL/CNRS/UNISTRA
5 rue du général Cassagnou
68301 Saint-Louis, France
**e-mail: lucia.blas@isl.eu*

[b] *S. Braun*
French-German Institute of Research of Saint-Louis
5 rue du général Cassagnou
68301 Saint-Louis, France

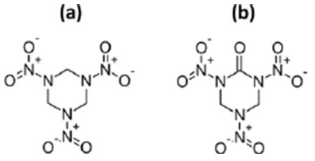

Figure 1. Chemical structure of RDX (a) and K6 (b).

Keto-RDX (2-oxo-1,3,5-trinitro-1,3,5-triazacyclohexane, K6) is a very powerful energetic material among nitro-urea explosives. Structurally similar to the well-known RDX, which is 1,3,5-trinitroperhydro-1,3,5-triazine (see Figure 1). K6 appears to be an interesting explosive considering its several physical properties and thermal characteristics, like 4% more enthalpy of reaction than HMX (at early times of reaction and at the same relative density) [21,22]. Moreover, it can be prepared from cost-effective starting materials. However, its main drawback is a high sensitivity, particularly in terms of impact sensitivity (< 1.56 J).

In order to reduce the sensitivity of K6, two different methods were investigated within this work. First, the nanocrystallization of K6 by the SFE process, and second, the simultaneous crystallization of n-K6/n-RDX mixture. The latter has not been studied before in the literature. The SFE process offers the possibility of producing homogeneous mixtures that cannot be obtained by other methods (as physical mixture and milling). Moreover, most of other explosive mixtures have been used only in micrometric size.

Sensitivity tests were performed on raw materials and as obtained products to compare results and conclude.

2 Experimental Section

2.1 Synthesis

Nano-K6 and physical mixtures of n-K6/n-RDX were prepared by the Spray Flash Evaporation (SFE) technique. This process is based on flashing behavior of superheated liquids that are subject to a high pressure drop. The compounds intended to be crystallized are dissolved in a low boiling solvent (acetone in this case). Acetone was of HPLC grade, used as received from Sigma Aldrich and without any further purification. The solution is exposed to an overpressure of 4 to 6 MPa and afterwards it is atomized into an evacuated chamber using a heated hollow cone nozzle (140 °C). Pressure inside the atomization chamber is maintained at around 500 Pa by means of a 35 $m^3 h^{-1}$ vacuum pump. The immense and sudden strong pressure drop that undergoes the liquid displaces the thermodynamic equilibrium. Pressure and boiling temperature decrease, therefore the solution becomes thermodynamically unstable and supersaturation occurs. During this metastable state, the superheated liquid strives to attain its thermodynamic stable state by removal of energy. The excess thermal energy is converted to latent energy, triggering an ultrafast evaporation of the solvent, supersaturation, as mentioned above, and consecutive nucleation and crystallization of the solute. The strong temperature drop accompanying the evaporation (from 140 °C to −30 °C) has a protective effect on the nanoparticles preventing them from further growth. Particles are retrieved from the gas flow using two axial cyclones placed in parallel inside the setup. Parameters used in these experiments are listed in Table 1. The yield corresponds to the quantity of n-K6 obtained after SFE process reported to the quantity of the raw, sub-millimeter (smm)-K6 dissolved in acetone.

Table 1. Crystallization experimental conditions.

	n-K6	n-K6/n-RDX	
Molar ratio	Pure K6	1:1	2:1
Solvent	Acetone	Acetone	Acetone
Masses [g]	2.02	1 g K6 0.94 g RDX	1 g K6 0.47 g RDX
Solute concentration [%]	1	1	1
Solution volume [mL]	250	240	184
Nozzle temperature [°C]	140	140	140
Cyclone temperature [°C]	80	80	80
Nozzle diameter [μm]	80	80	80
Pressure [MPa]	4	4	4
Duration [min]	19	31	16
Product [g]	0.77	1.06	0.78
Yield [%]	38	54	53

Smm-K6 with a purity of 95% was obtained by a first cyclization of formaldehyde, *tert*-butylamine and urea to 2-oxo-5-tert-butyl-1,3,5-triazacyclohexane. Afterwards, this product was nitrated to K6 with a mixture of acetic acid anhydride and nitric acid. The crude product was recrystallized from boiling ethyl acetate [23,24]. Particle size distribution is in the range from 0.4 to 1.2 mm (derived from sieves analysis – not shown here).

2.2 Analysis

X-ray Powder Diffraction (XRD) measurements were performed with a Bruker AXS Advance D8 (Karlsruhe, Germany) X-ray diffractometer in Bragg-Brentano setup using K_α radiation ($\lambda(K_\alpha) = 1.54$ Å) at an acceleration voltage of 40 kV and 40 mA working current.

AFM patterns were recorded by means of a MultiMode Nanoscope IV configuration from the Bruker Metrology Group (Santa Barbara, USA) equipped with a Bruker "RTESP" (Rotated Tip Etched Silicon Probe) AFM probe. The probe has a silicon cantilever with a length of 125 mm, a width of 35 mm, and a thickness of 4 mm. The tip has a curvature radius of about 10 nm. For AFM analysis n-K6 or n-K6/n-RDX pellets were used. The 4 mm diameter and about 2 mm height pellet was pressed with a pressure of 100 MPa. In order to have a pellet with a regular surface, around 200 μm were scraped using a Leica RM microtome. The last cutting steps were performed at 1 μm. The median roughness of the obtained surface was about ±100 nm. The material was observed at room temperature and at-

mospheric pressure. AFM images of $2.5 \times 2.5\ \mu m$ (see Figure 3 and Figure 7) were used. By measuring q_2 (area) of around 1000 particles and considering them spherical to obtain their diameter, an accurate particle size distribution was obtained.

DSC measurements were performed with a Q1000 from TA Instruments (New Castle, USA) at atmospheric conditions, under 50 mL min^{-1} in an argon atmosphere and with a heating rate of 5 K min^{-1}.

NMR measurements were performed with a 400-MHz NMR spectrometer from Agilent Technologies (Santa Clara, USA), under the following conditions: frequency was 399.685 Hz, number of scans was 8, temperature was 25 °C, acquisition time was 1.861 s, and recycle delay (d1) was 2.0 s.

Sensitivity towards initiation by impact, friction, and electrostatic discharge (ESD) were performed according to the BAM (Bundesanstalt für Materialprüfung, Berlin, Germany) guidelines (www.bam.de).

3 Results and Discussion

3.1 K6 Nanocrystallization

Nano-K6 was prepared using the SFE technique. Due to a good solubility of K6 in acetone, the latter was chosen as solvent. Moreover, acetone is thermally stable to a large extent and offers low toxicity. Smm-K6 was obtained previously by a two-step synthesis method with a purity of 95% (see Experimental Section) [23, 24].

X-ray diffraction analysis was performed on the obtained n-K6 product in the range of $2\theta = 10$ to 40° (see Figure 2).

Results reveal that obtained n-K6 is crystalline, and crystallizes as an orthorhombic crystal system [25]. n-K6 shows an identical diffraction signature compared to the one obtained by simulation with Mercury CSD 2.0 software [26]. Moreover, mean crystallite size was calculated from the well-known Scherrer equation [27] with a shape factor of 0.89, using the full width at half maximum intensity (FWHM) of the X-ray signals of smm-K6 and n-K6 samples. Results revealed a decrease in crystallites size from 80 nm (smm-K6) to 40 nm (n-K6). Therefore, the smm-K6 raw material tends to be extremely polycrystalline (since absolute lengths are in the millimeter range, see Experimental Section), whereas the nanomaterial shows much less defects like grain boundaries that can interrupt coherence of the X-ray beam. Anyhow, the detected coherence in case of the nanomaterial is smaller than absolute sizes from AFM (see Figure 3, next section) – so only a small amount (19%) of the nanomaterial is claimed to be really monocrystalline.

Particle size distribution of n-K6 was measured by Atomic Force Microscopy (AFM). The median particle size (x_{mean}) is about 74 nm (see Figure 3).

Thermal studies were performed on prepared n-K6 and on raw smm-K6 (see Figure 4). smm-K6 and n-K6 decompose both without melting within a narrow temperature range. The decomposition peak of n-K6 shows a maximum at 175 °C, whereas smm-K6 provides a maximum at 187 °C. As observed before, when decreasing the particles size of energetic materials, the decomposition temperature decreases [28, 29]. The latter can be easily explained by a higher surface to volume ratio of smaller particles and the linked chemical and physical activity of molecules/atoms at the surface of the particles in contrast to decreased activity of atoms inside the volume. Energy evolved

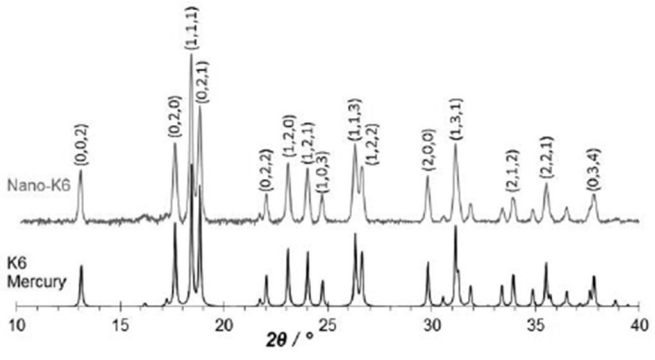

Figure 2. X-ray Diffraction patterns of n-K6 obtained by SFE process and simulated by the Mercury CSD 2.0 software.

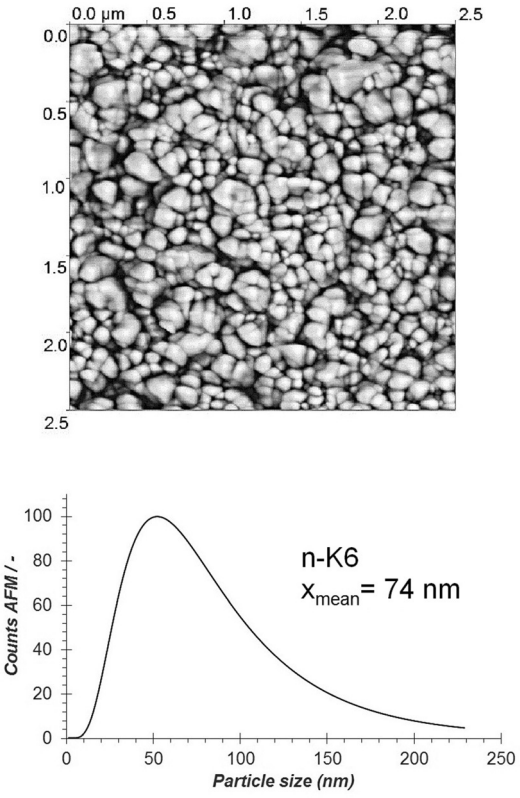

Figure 3. AFM image (top) and particle size distribution (bottom) for n-K6 obtained by measuring the surface exposed area of around 1000 particles from AFM images.

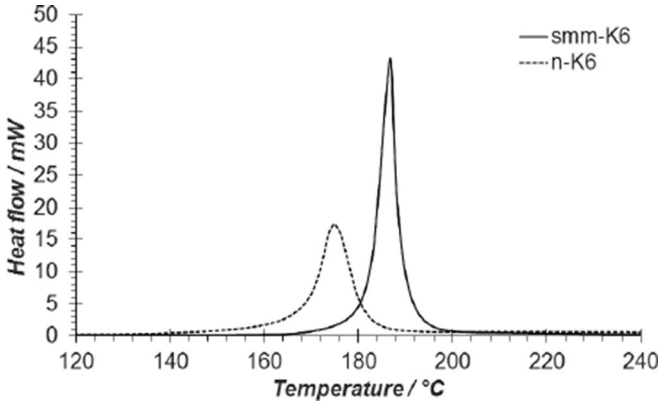

Figure 4. DSC curves of smm-K6 (solid line) and n-K6 (dotted line).

in decomposition reaction was calculated by DSC curves integration (between 140 and 195 °C for n-K6 and between 160 and 205 °C for smm-K6). Hence, following results are given: 2567 $J g^{-1}$ for smm-K6 and 2073 $J g^{-1}$ for n-K6. These values are in line with the one measured by Sikder et al. for a μ-K6 sample (2303 $J g^{-1}$) [21]. In this work Sikder et al. prepared μ-sized material from a batch process and claim K6 as the most powerful energetic material among nitrourea explosives that only can be used in phlegmatized version.

Furthermore sensitivity tests were performed on smm-K6 from batch synthesis and n-K6 obtained by the SFE process. Sensitivity to friction and electrostatic discharge can be intensively reduced (33 % and 24 %, respectively) by scaling down the particle size distribution of K6 from sub-millimeter size to nanosize (see Table 2). Impact sensitivities of

Table 2. Impact, friction, and ESD sensitivities of smm-K6, n-K6, μ-RDX, n-RDX, and n-K6/n-RDX.

	Impact sensitivity [J]	Friction sensitivity [N]	ESD [J]
smm-K6	< 1.56	48	0.120
n-K6	< 1.56	72	0.158
μ-RDX	3.52	160	0.119
n-RDX	2.05	180	0.359
n-K6/n-RDX	3.03	168	0.246

both smm-K6 and n-K6 are undergoing the limit of detection of the fall hammer device that was used for this study (< 1.56 J, see Experimental Section). Therefore it is not possible to conclude in terms of the influence of the particle size of K6 on its impact sensitivity.

From these results, it can be concluded that n-K6 cannot be used in civil or military applications, because of its high sensitivity to impact, which makes the material not safe to be handled. This result, in accord with Sikder at al. [21], shows one more time the specific high interest to desensitize K6. Therefore a K6 and RDX mixed solution (processed via SFE) was investigated within the following section.

In this context, Shokrolahi et al. produced n-K6 by spraying a solution of K6-acetone into an antisolvent, namely water [29]. Their results show that K6 impact and friction sensitivity is decreased of 16 % by reducing the K6 particles size from micro-size to around 60 nm. Decrease in friction sensitivity is in good agreement (16 % vs. 33 % from present work) with results demonstrated in this study.

3.2 Nanocrystallization of a K6 and RDX Mixture by Spray Flash Evaporation (SFE)

In order to reduce K6 sensitivity, the possibility of producing a cocrystal between K6 and RDX was studied. The molecule of K6 is similar to the one of RDX, finally, it is a keto-derivative of RDX (see Figure 1). In fact, the possibility of forming a cocrystal by electrostatic interaction of the ketone oxygen of K6 with a hydrogen atom of the RDX heterocycle was investigated. With this objective, a 1:1 molar ratio mixture of n-K6/n-RDX was crystallized by SFE.

The synthesized product (n-K6/n-RDX mixture) was yellowish, while raw materials were all white. Since impurities and the formation of a cocrystal can be excluded (to be presented below) the color could be a result of molecular interaction between the K6 and RDX molecules at the particles surface. However, a focus on this phenomenon would be a complete different topic and could be investigated by DFT calculations regarding the molecular interactions between K6-RDX surfaces. The latter could lead to a slight absorption of the bluish regime from the VIS spectrum that leads to above mentioned yellow color.

NMR spectroscopy studies (not shown here) were performed on the material and verified that the 1:1 molar proportion was maintained during SFE process. The material was further analyzed by X-ray Powder Diffraction (XRD) to investigate a possible cocrystal-formation. According to the results obtained by XRD (presented in Figure 5), no cocrys-

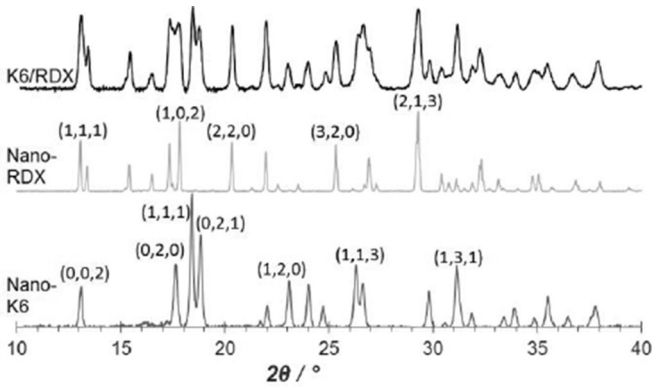

Figure 5. From top to bottom: X-ray Diffraction patterns of 1:1 molar ratio n-K6/n-RDX mixture produced by the SFE process, n-RDX, and n-K6.

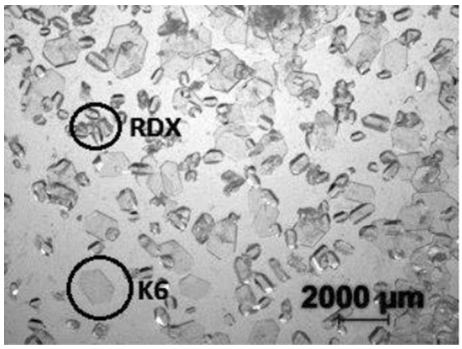

Figure 6. Image from an optical microscope depicting RDX and K6 crystals in the micrometer range produced by slow evaporation.

tal formation was revealed. The XRD pattern of the n-K6/n-RDX mixture does not present any new reflexes which would be a strong hint for the formation of a new co-crystalline network. Only characteristic signals of pure K6 (orthorhombic crystal system) and pure RDX (alpha phase, orthorhombic crystal system [30]) were observed. The same study was performed with a molar ratio of 2 : 1 K6/RDX, in this case the formation of a cocrystal was neither observed.

The mean volume-weighted domain sizes of K6 and RDX in the mixture was calculated by the Rietveld method as implemented in the Fullprof software [31]. This method allows the refinement of structural information, microstructural (size and strain effects) and instrumental parameters by minimizing the weighted sum of the squared differences between the observed and the calculated powder pattern. Due to the complexity of the pattern, atomic positions could not be fitted. However, calculations from refinements give an approximation of the mean crystallite size, which is between 45–50 nm for RDX and 40–45 nm for K6.

In parallel, a slow evaporation crystallization of a mixture of K6 and RDX dissolved in acetone was carried out. The aim of this experiment was to verify, if under these conditions (slow solvent evaporation rate) a cocrystal formation is detected. As observed before by SFE, both compounds crystallized separately (see Figure 6 obtained with an optical microscope). Single crystal diffraction studies were performed on the two different types of crystals produced to identify them. Larger and flat crystals with hexagonal morphology correspond to K6 (orthorhombic) and smaller, prismatic crystals correspond to RDX (α-phase, orthorhombic).

From this study, it was shown that there is no formation of a K6/RDX cocrystal (neither by SFE nor slow evaporation). The SFE process renders possible production of a homogeneous mixture of n-K6/n-RDX, with different properties compared to the ones of single raw materials, as it will be shown afterwards.

The particle size distribution of the n-K6/n-RDX mixture (produced by SFE) was studied by AFM, following the method described above for n-K6 (see Experimental Section). AFM image is shown in Figure 7. From that a median particle size x_{mean} about 82 nm was derived.

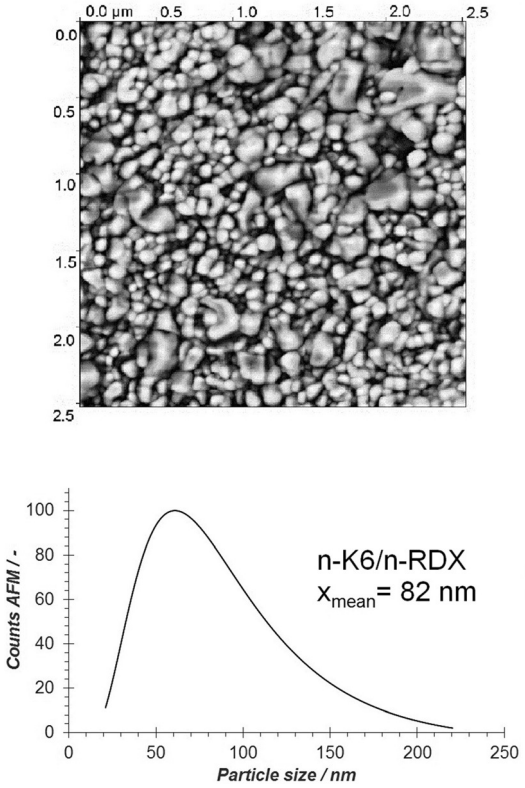

Figure 7. AFM image and particle size distribution for n-K6/n-RDX mixture.

The performance of this mixture was studied in terms of sensitivity. Results are shown in Table 2. Sensitivities show that the mixture offers friction sensitivity and electrostatic discharge sensitivity between the one of both pure explosives. Moreover, the mixture n-K6/n-RDX is less sensitive to impact than the pure materials.

As it can be observed in Table 2, scaling down particle sizes of RDX consequently increases its impact sensitivity from 3.52 J to 2.05 J. For K6, even if it was not possible to measure the sensitivity (both below the limit of detection), smm-K6 was statistically less sensitive than n-K6 (5 negative tests before one positive test). However, when the molecules are crystallized in a n-K6/n-RDX mixture, they are less sensitive to impact than separately. This result becomes really interesting for future applications of composite nanomaterial.

The thermal response of the mixture was studied by DSC. Results are shown in Figure 8.

Two peaks of decomposition are examined: the first one shows a maximum at 174 °C and corresponds to K6 decomposition. The second one offers a maximum at 234 °C and corresponds to RDX decomposition. Moreover, an endothermic melting signal is observed before the first decomposition peak. That can be explained by a first decomposition of K6, which locally increases the temperature and

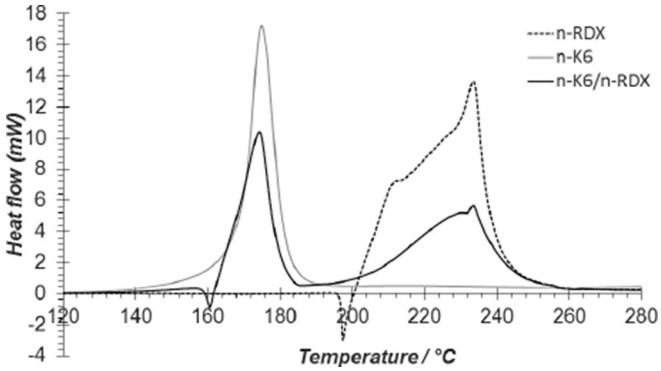

Figure 8. DSC curves of n-K6, n-RDX, and n-K6/n-RDX mixture obtained by SFE process.

supplies enough energy to melt RDX, therefore decomposition of K6 and melting of RDX take place at the same time. Energies evolved from decomposition reactions are 3758 $J g^{-1}$ for pure n-RDX (dotted line) and 3573 $J g^{-1}$ for RDX present in the mixture (n-K6/n-RDX, black solid line). In the case of K6 evolved energies correspond to 2073 $J g^{-1}$ for pure n-K6 (grey solid line) and 2352 $J g^{-1}$ for n-K6 present in the mixture (first peak between 162 and 185 °C, black solid line). Energy of K6 decomposition in the mixture (n-K6/n-RDX) is not exactly the same compared to the one evolved by pure n-K6. This observation can be partially explained by the fact that within the mixture the melting of n-RDX and the decomposition of n-K6 take place at the same time.

Results presented in this section revealed that even if K6/RDX cocrystal formation was not observed, there is a synergy between both particle phases present in the mixture. Consequently, the behavior of the mixture is different from the one of the pure materials (in terms of sensitivity; thermal behavior and even color). Scanning Electron Microscopy (SEM) analyses were performed (not shown here) on the n-K6/n-RDX mixture. Results document the presence of only one type of particles (lack of a bimodal population), which presented the same behavior under the electron beam. These results suggested the possibility of a core-shell configuration, where K6 would be at the core and RDX at the surface of the particle (K6 is less soluble in acetone than RDX). Further studies will be performed to investigate this hypothesis. For this, new analysis techniques will be optimized in our laboratory.

4 Conclusions

In this work two possible ways to reduce the sensitivity of K6 were studied. On the one hand, the crystallization of n-K6 by SFE was investigated. On the other hand, the production of a K6 and RDX composition was studied.

Nano-K6 with a particle size around 74 nm was successfully crystallized by SFE. By reducing K6 particle size, it became less sensitive to friction and electrostatic discharge. Moreover, n-K6 decomposes at lower temperature than smm-K6. However, it cannot be used in civil or military applications due to its high sensitivity to impact ($<$ 1.56 J).

The possibility of forming a cocrystal between K6 and RDX by SFE was studied. Under present experimental conditions no formation of a cocrystal was observed. Regardless, a homogeneous mixture of K6/RDX at the nanoscale was achieved by SFE. The mixture has low friction and ESD sensitivities, with a view to the ones of the individual raw materials. Interestingly, n-K6/n-RDX mixture is less sensitive to impact (3.03 J) than the raw compounds separately (n-RDX 2.05 J and n-K6 $<$ 1.56 J).

The Spray Flash Evaporation is an innovative process allowing the continuous production of nano-energetic materials and physical mixtures of different materials. Finally, a novel mixture of explosives (n-K6/n-RDX) at the nanoscale with interesting properties in terms of performances and sensitivities could be demonstrated.

Symbols and Abbreviations

AFM – Atomic Force Microscopy
DSC – Differential Scanning Calorimetry
ESD – Electrostatic Discharge
NMR – Nuclear Magnetic Resonance Spectroscopy
SEM – Scanning Electron Microscopy
SFE – Spray Flash Evaporation
smm – Sub-millimeter
XRD – X-ray diffraction

Acknowledgments

Authors would like to thank Ms. Nathalie Gruber of the Molecular Tectonics Laboratory (UMR 7140, Strasbourg, France) for performing Single Crystal Diffraction and for obtaining photographs of K6/RDX crystals in an optical microscope.

References

[1] C. Rossi, Two Decades of Research on Nano-Energetic Materials, *Propellants Explos. Pyrotech.* **2014**, *39*, 323–327.
[2] D. Spitzer, M. Comet, C. Baras, V. Pichot, N. Piazzon, Energetic Nano-materials: Opportunities for Enharced Performances, *J. Phys. Chem. Solids* **2010**, *71*, 100–108.
[3] X. Song, Y. Wang, C. An, X. Guo, F. Li, Dependence of Particle Morphology and Size on the Mechanical Sensitivity and Thermal Stability of Octahydro-1,3,5,7-tetranitro-1,3,5,7-tetrazocine, *J. Hazard. Mater.* **2008**, *159*, 222–229.
[4] X. Song, Dependence of Particle Size and Size Distribution on Mechanical Sensitivity and Thermal Stability of Hexahydro-1,3,5-trinitro-1,3,5-triazine, *Def. Sci. J.* **2009**, *59*, 37–42.
[5] V. Stepanov, L. N. Krasnoperov, I. B. Elkina, X. Zhang, Production of Nanocrystalline RDX by Rapid Expansion of Supercritical Solutions, *Propellants Explos. Pyrotech.* **2005**, *30*, 178–183.

[6] D. Spitzer, C. Baras, M. R. Schäfer, F. Ciszek, B. Siegert, Continuous Crystallization of Submicrometer Energetic Compounds, *Propellants Explos. Pyrotech.* **2011**, *36*, 65 – 74.
[7] R. Kumar, P. F. Siril, P. Soni, Preparation of Nano-RDX by Evaporation Assisted Solvent-Antisolvent Interaction, *Propellants Explos. Pyrotech.* **2014**, *39*, 383 – 389.
[8] C. An, H. Li, W. Guo, X. Geng, J. Wang, Nano Cyclotetramethylene Tetranitramine Particles Prepared by a Green Recrystallization Process, *Propellants Explos. Pyrotech.* **2014**, *39*, 701 – 706.
[9] J. Liu, W. Jiang, F. Li, L. Wang, J. Zeng, Q. Li, Y. Wang, Q. Yang, Effect of Drying Conditions on the Particle Size, Dispersion State, and Mechanical Sensitivities of Nano HMX, *Propellants Explos. Pyrotech.* **2014**, *39*, 30–39.
[10] B. Risse, F. Schnell, D. Spitzer, Synthesis and Desensitization of Nano-β-HMX, *Propellants Explos. Pyrotech.* **2014**, *39*, 397–401.
[11] J. Li, T. B. Brill, Nanostructured Energetic Composites of CL-20 and Binders Synthesized by Sol Gel Methods, *Propellants Explos. Pyrotech.* **2006**, *31*, 61–69.
[12] Y. Bayat, V. Zeynali, Preparation and Characterization of Nano-CL-20 Explosive, *J. Energ. Mater.* **2011**, *29*, 281–291.
[13] P. Redner, D. Kapoor, R. Patel, M. Chuang, D. Martin, Production and Characterization of Nano-RDX, *U.S. Army Science Conference*, **2006**.
[14] A. Pivkina, P. Ulyanova, Y. Frolov, S. Zavyalov, J. Schoonman, Nanomaterials for Heterogeneous Combustion, *Propellants Explos. Pyrotech.* **2004**, *29*, 39 – 48.
[15] N. Radacsi, A. I. Stankiewicz, Y. L. M. Creyghton, A. E. D. M. van der Heijden, J. H. ter Horst, Electrospray Crystallization for High-Quality Submicron-Sized Crystals, *Chem. Eng. Technol.* **2011**, *34*, 624 – 630.
[16] B. Risse, D. Spitzer, and D. Hassler, Preparation of Nanoparticles by Flash Evaporation, Patent WO 2013/117671 A1, **2013**.
[17] B. Risse, D. Spitzer, D. Hassler, F. Schnell, M. Comet, V. Pichot, H. Muhr, Continuous Formation of Submicron Energetic Particles by the Flash-Evaporation Technique, *Chem. Eng. J.* **2012**, *203*, 158 – 165.
[18] D. Spitzer, B. Risse, F. Schnell, V. Pichot, M. Klaumünzer, M. R. Schaefer, Continuous Engineering of Nano-Cocrystals for Medical and Energetic Applications, *Sci. Rep.* **2014**, *51*, 4.
[19] R. Meyer, J. Köhler, A. Homburg, *Explosives*, Wiley-VCH, Weinheim **2007**.
[20] R. N. Rogers, Incompatibility in Explosive Mixtures. Detection of Thermally Hazardous Explosives Mixtures, *Ind. Eng. Chem. Prod. Res. Dev.* **1962**, *1*, 169 – 172.
[21] N. Sikder, N. R. Bulakh, A. K. Sikder, D. B. Sarwade, Synthesis; Characterization and Thermal Studies of 2-Oxo-1,3,5-trinitro-1,3,5-triazacyclohexane (Keto-RDX or K-6), *J. Hazard. Mater.* **2003**, *96*, 109–119.
[22] A. R. Mitchell, P. F. Pagoria, C. L. Coon, E. S. Jessop, J. F. Poco, C. M. Tarver, R. D. Breithaupt, G. L. Moody, Nitroureas 1. Synthesis Scale-up and Characterization of K-6, *Propellants Explos. Pyrotech.* **1994**, *19*, 232–239.
[23] H. Ritter, S. Braun, F. Ciszek *Neue Explosivstoffe für Hochleistungs-LOVA-Munition*. 4. Formulierungen mit K-6. CR/RV 443/2003, **2003**.
[24] H. Ritter, Relationship Between Crystal Shape and Explosive Properties of K-6, *32th International Annual Conference of ICT Energetic Materials*, Karlsruhe, FRG, Germany, July 3–6, **2001**.
[25] R. Gilardi, J. L. Flippen-Anderson, C. George, Structures of 1,3,5-Trinitro-2-oxo-1,3,5-triazacyclohexane (I) and 1,4-Dinitro-2,5-dioxo-1,4-diazacyclohexane (II), *Acta Crystallogr., Sect. C* **1990**, *46*, 706–708.
[26] C. F. Macrae, P. R. Edgington, P. McCabe, E. Pidcock, G. P. Shields, R. Taylor, M. Towler, J. van de Streek, Mercury: Visualization and Analysis of Crystal Structures, *J. Appl. Crystallogr.* **2006**, *39*, 45–457.
[27] P. Scherrer, Bestimmung der Größe und der inneren Struktur von Kolloidteilchen mittels Röntgenstrahlen, *Göttinger Nachrichten Math. Phys.* **1918**, *2*, 98 – 100.
[28] M. R. Sovizi, S. S. Hajimirsadeghi, B. Naderizadeh, Effect of Particle Size on Thermal Decomposition of Nitrocellulose, *J. Hazard. Mater.* **2009**, *168*, 1134–1139.
[29] A. Shokrolahi, A. Zali, A. Mousaviazar, M. H. Keshavarz, H. Hajhashemi, Preparation of Nano-K-6 (Nano-Keto RDX) and Determination of Its Characterization and Thermolysis, *J. Energ. Mater.* **2011**, *29*, 115–126.
[30] C. S. Choi, The Crystal Structure of Cyclotrimethylenetrinitramine, *Acta Crystallogr., Sect. B* **1972**, *28*, 2857 – 2862.
[31] J. Rodríguez-Carvajal, FULLPROF: a Program for Rietveld Refinement and Pattern Matching Analysis, *Abstracts of the Satellite Meeting on Powder Diffraction of the XV Congress of the IUCr*, Toulouse, France, **1990**, p. 127.

Received: July 17, 2015
Revised: September 15, 2015
Published online: October 14, 2015

